Structural Relaxation of Stacked Ultrathin Polystyrene Films

YUNG P. KOH, SINDEE L. SIMON

Department of Chemical Engineering Texas Tech University Lubbock, Texas 79409-3121

Received 15 June 2008; revised 10 September 2008; accepted 21 September 2008
DOI: 10.1002/polb.21598
Published online in Wiley InterScience (www.interscience.wiley.com).

ABSTRACT: The T_g depression and kinetic behavior of stacked polystyrene ultrathin films is investigated by differential scanning calorimetry (DSC) and compared with the behavior of bulk polystyrene. The fictive temperature (T_f) was measured as a function of cooling rate and as a function of aging time for aging temperatures below the nominal glass transition temperature (T_g). The stacked ultrathin films show enthalpy overshoots in DSC heating scans which are reduced in height but occur over a broader temperature range relative to the bulk response for a given change in fictive temperature. The cooling rate dependence of the limiting fictive temperature, T_f', is also found to be higher for the stacked ultrathin film samples; the result is that the magnitude of the T_g depression between the ultrathin film sample and the bulk is inversely related to the cooling rate. We also find that the rate of physical aging of the stacked ultrathin films is comparable with the bulk when aging is performed at the same distance from T_g; however, when conducted at the same aging temperature, the ultrathin film samples show accelerated physical aging, that is, a shorter time is required to reach equilibrium for the thin films due to their depressed T_g values. The smaller distance from T_g also results in a reduced logarithmic aging rate for the thin films compared with the bulk, although this is not indicative of longer relaxation times. The DSC heating curves obtained as a function of cooling rate and aging history are modeled using the Tool-Narayanaswamy-Moynihan model of structural recovery; the stacked ultrathin film samples show lower β values than the bulk, consistent with a broader distribution of relaxation times. J Polym Sci Part B: Polym Phys 46: 2741–2753, 2008
Keywords: ageing; glass transition; nanolayers; polystyrene; thin films

INTRODUCTION

The effects of nanoconfinement on the glass transition phenomena of polymer materials have been extensively investigated, and several review articles have been recently written.[1–3] Although the experimental results in the literature seem to depend on the measurement technique and material studied, it is generally accepted that the glass transition temperature (T_g) of polymer ultrathin films is depressed relative to the bulk unless strong interactions with a substrate are present. For example, both supported and unsupported (free standing) polystyrene ultrathin films show a noticeable T_g depression relative to that of the bulk state.[4–23] For polystyrene, the magnitude of depression can be as great as 70 °C in freely standing ultrathin films.[6] In addition, Ellison and Torkelson's work[9] on labeled layers in supported polystyrene films shows that there is a gradient in the T_g depression with a greater depression at the surface and only a small depression at the polystyrene/glass substrate interface.

It is well recognized that the glass transition temperature occurs when the time scale of

Correspondence to: S. L. Simon (E-mail: sindee.simon@ttu.edu)

material relaxation and the time scale of measurement are comparable. The relationship between the relaxation time, the cooling rate, and the glass transition temperature can be derived as follows: [24]

$$\frac{d\tau}{dt} = \frac{d\tau}{dT}\frac{dT}{dt} = -\frac{\Delta h}{RT_g^2} q\tau = 1 \quad (1)$$

where τ is the relaxation time at T_g, t is the measurement time, Δh is the effective activation energy at T_g, defined as $(d\ln \tau/d(1/T))$ at T_g, R is the gas constant, and q is the cooling rate. A relaxation time of 10 s is approximately equivalent to the measurement time scale when cooling at 10 K/min for $\Delta h/RT_g^2 = 0.7$. For polymers, the value of $\Delta h/RT_g^2$ is 0.72 ± 0.07;[25] the value differs for other types of materials.[24,25]

The time scale of measurement has been also shown to influence the magnitude of the T_g depression at the nanoscale because the dependence of T_g on the time scale of measurement (i.e., the effective activation energy) differs between bulk and nanoscale materials. Schonhals et al.[26] reported that the average relaxation time as measured by dielectric spectroscopy in nanopore-confined poly(methyl phenyl siloxane) (PMPS) has a weaker temperature dependence than the bulk, with the slope of log τ versus temperature decreasing to ~15% of the bulk at 2.5 nm nanopore confinement. As a result, the average relaxation time is reduced significantly under nanopore confinement at lower temperatures, whereas at higher temperatures, the relaxation time is greater for the nanoconfined material. On the other hand, Fakhraai and Forrest[7] found that the T_g depression is inversely proportional to the cooling rate, and the T_g of the ultrathin films approaches that of the bulk at a cooling rate of 130 K/min in supported polystyrene ultrathin films. Both Schonhals' and Fakhraai's works[7,26] reveal that the timescale of measurement influences the magnitude of T_g depression, perhaps explaining why no discernable T_g depressions were found in nanocalorimetry[18,19] and AC calorimetry studies[20] for polystyrene films as thin as 3 nm due to the high cooling rates and the high frequencies used in those studies.

In addition to affecting the dynamics of the glass transition, nanoconfinement also is expected to influence the kinetics of structural relaxation in the glassy state. However, the effects of the nanoconfinement on physical aging have not been well studied, and some of the results are seemingly contradictory.[21,22,27–29] Both acceleration and retardation of structural relaxation during physical aging were reported for different types of nanoconfinement and materials. Acceleration is observed for small molecules confined in nanopores because the equilibrium state below T_g differs under this type of nanoconfinement due to isochoric vitrification resulting in smaller relaxation times at temperatures a given distance below T_g.[27] In contrast, physical aging is observed to be slower in PMMA ultrathin films compared with the bulk presumably because attractive interactions between the ester groups of PMMA and the hydroxyl group of the silica substrate restrict physical aging of PMMA ultrathin films supported on silica substrate.[28] On the other hand, the rate of aging of a 20 nm polystyrene ultrathin film is suggested to be similar to that of the bulk far below T_g for aging times up to 80 min, whereas at an aging temperature just below the bulk T_g, the thin film does not age because it is in the equilibrium state due to its T_g depression.[29] Other early work on aging of polystyrene ultrathin films showed depressed enthalpy overshoots compared with bulk, but the aging rates were not quantified.[21] In addition to the aging behaviors of ultrathin films, the aging of submicron thin films of polysulfone and poly(2,6-dimethyl-1,4-phenylene oxide) was investigated for aging times of more than 200 days at aging temperature more than 130 °C below T_g using gas permeability and refractive index.[30,31] The aging rate of the thin films (in terms of the slope of log permeability versus log t) increases with decreasing film thickness and with increasing aging temperature in spite of the fact that the T_gs of the submicron-thick thin films are unchanged from the bulk.[31]

The dynamics and T_g depression in polymer ultrathin films have also been suggested to be related to those in polymer nanocomposites.[32,33] Although nanocomposites differ from supported ultrathin films in that their confinement may be three-dimensional and due to presence of multiparticle interactions, the effects of film thickness and interparticle spacing on T_g have been related.[32,33] Hence, the physical aging of nanocomposites may also be similar to that of the ultrathin films. Unlike ultrathin films, the physical aging of nanocomposites, especially for thermosetting resins, has been more extensively investigated.[34–38] The studies of physical aging of nanocomposites have focused on the type of nanofiller, such as silica nanoparticle, graphitic nanofiber, and polyhedral oligosilsesquioxane (POSS),

because strong interactions between nanofiller and the thermosetting resin appear to restrict physical aging.[34] Similarly, in the case of ultrathin films, interfacial interactions may be an important factor for their physical aging behavior.

In our previous work, the T_g depression and absolute heat capacity of stacked ultrathin polystyrene film samples were reported.[23] The advantage of using stacked ultrathin films to study nanoconfinement and intrinsic size effects is that the films do not have free surfaces after annealing above T_g but rather are assumed to have neutral polystyrene–polystyrene interfaces. Multilayer films were also made by Ellison and Torkelson[9] to investigate how the T_g of a thin layer depended on its location in the film (e.g., at the surface, substrate, or in the interior of the film) and how it depended on the chemical structure of the adjoining layers.[39] The interior layer was found to exhibit a bulk-like T_g when both over and under layers had bulk-like thicknesses, whereas for bilayer and trilayer films composed of two or three ultrathin films, T_g depressions were observed although in the trilayer film, the depression was greater at the surface and weaker at the substrate.[9] The results of the bilayer and trilayer stacks of ultrathin films showed that a gradient in T_g exists. Moreover, it was suggested that the average T_g in the bilayer and trilayer ultrathin film stacks was similar to that displayed by single films having the same total thicknesses—thus, suggesting that a stack of ultrathin films should show bulk T_g behavior if the stack is thick enough. This is contrary, however, to our observation that stacked ultrathin film samples containing more than 200 ultrathin films show T_g depressions of similar magnitude to those observed for supported thin films.[23] Our results are not inconsistent, though, with Torkelson et al.'s observation that the T_g of a layer depends on the T_g of the layers around it—in our case, these layers are all ultrathin films seemingly with the same depressed T_gs such that the T_g measured is that of a single layer with no free surface and neutral interactions.

It is important to note that the polystyrene used in our stacked samples is ultrahigh molecular weight in order that diffusion between layers cannot occur in the time scale of the experiments such that each film in the stack retains its ultrathin film character; in fact, when interlayer diffusion is allowed to occur (with annealing at high temperature in a press), T_g reverts back to the bulk value as would be expected.[23] In our previous work, we not only found a T_g depression similar to that reported for supported polystyrene films,[4,5] but in addition, we found a decrease in the absolute heat capacity in both liquid and glassy regions at the nanoscale. The step in heat capacity at T_g, ΔC_p, was also found to decrease with decreasing film thickness. Here, we add to our previous results and extend the study to measure the calorimetric glass transition temperature of the stacked polystyrene ultrathin films as a function of cooling rate and to investigate the physical aging behavior of the ultrathin film samples. In addition to examining the kinetics associated with T_g in these samples, the Tool-Narayanswamy-Moynihan (TNM) model of structural recovery[40–42] is employed to allow the quantitative comparison and physical interpretation of the results. The TNM model is widely used to describe the glass transition kinetics of glass-forming materials[24,43–47] even though it is known to have shortcomings.[24,48] In this work, we will use it to help us quantify differences in the nonexponentiality and nonlinearity, by the parameters of β and x, in the ultrathin film and bulk samples.

METHODOLOGY

Sample Preparation

The polystyrene used in this study, obtained from Sigma-Aldrich, has a number–average molecular weight of 1,998,000 g/mol and a molecular weight distribution of 1.02. The radius of gyration (R_g) is 38.7 nm.[49] Polystyrene ultrathin films were deposited by spin coating polystyrene dissolved in toluene (HPLC-grade; Sigma-Aldrich) onto freshly cleaved 1-in^2 mica substrates. In our previous work, film thicknesses were found to range from 17.3 to 97.0 nm (based on atomic force microscope measurements) for polystyrene/toluene solutions ranging from 0.4 to 1.5 weight % polymer. Here, we used concentrations of 0.8 and 0.5% to yield films of 61.5 and 38.0 nm (which are referred to hereafter as 62 and 38 nm films). After the spin coating, the films were removed from the mica substrate by floating onto water and then collecting on a Teflon plate. Films were continually stacked until the weight was enough for a differential scanning calorimetry (DSC) sample. About 200 ultrathin films were stacked to obtain one 3–5 mg weight of DSC sample. Finally, the film was removed from the Teflon plate using a razor blade. To remove any residual solvent and/or adventitious water, the stacked ultrathin film samples

were stored under the ambient conditions for 24 h and then annealed *in vacuo* at 50 °C and 5 Torr for 12 h prior to crimping the DSC pans. The same polystyrene sample in bulk was also studied.

DSC Measurements

The absolute heat capacity is measured by Perkin–Elmer Pyris 1 DSC with an ethylene glycol cooling system maintained at 5 °C in step scan mode, which consists of multiple temperature ramp/isothermal steps. The measurements are made on heating after first cooling the sample from 135 °C at 30 K/min; the methodology consists of 0.8 min isothermal holds every 2 K with 10 K/min ramps between temperatures. Calibration is performed using the same thermal history with sapphire, and this methodology was shown to give reliable measurements of absolute heat capacity in our previous study.[23] T_g was obtained from the absolute C_p versus temperature data using the half-height method; that is, the temperature at which C_p attains a value halfway between the extrapolated liquid and glassy values is taken to be T_g. Sample sizes were 5.57 and 2.97 mg for the 62 and 38 nm ultrathin films, respectively. For the bulk, five different samples, reported in previous work,[23] were used, ranging in size from 1.93 to 12.97 mg. The standard deviation of T_g for the bulk is ±0.2 K, independent of sample size.

In addition to using step scan, heating scan experiments were also performed in the Pyris1 DSC with ethylene glycol cooling system using the same stacked ultrathin film samples and different samples for the bulk. In one type of experiment, we measured the fictive temperature (T_f) on heating at a rate of 10 K/min after cooling at various rates, whereas in a second type of experiment, we measured the fictive temperature (T_f) as a function of aging time after isothermal structural relaxation. The fictive temperature is determined by Moynihan et al.'s method[40] as the intersection of the extrapolated liquid and glass enthalpy lines. We note that when no isothermal aging occurs between the cooling and heating runs, as in the first type of experiment, the fictive temperature is termed the limiting fictive temperature (T_f'),[43] and its value is approximately equal to T_g.[47,50] All measurements and aging experiments were made in a nitrogen atmosphere.

Prior to all experiments, samples were heated to 135 °C and held for 3 min in the DSC to erase their thermal history. For the cooling rate experiments, samples were then cooled to 35 °C at cooling rates ranging from 0.01 to 30 K/min, and then immediately heated again to 135 °C to obtain T_f ($= T_f'$). For the aging experiments, samples were cooled at 30 K/min from 135 °C to the aging temperature (T_a), aged isothermally for aging times ranging from 0 to 1000 min, and then cooled to 35 °C at 30 K/min; the fictive temperature was then measured on the subsequent heating scan at 10 K/min. The aging temperatures ranged from $T_g - 15$ K to $T_g - 5$ K, with T_g taken to be the value measured using step scan. Following each scan of the aged sample, the sample was cooled at 30 K/min from 135 °C and then heated at 10 K/min without aging; this provided an internal standard for the experiments to ensure that the sample did not change in the course of the experiments. Based on these "unaged" runs, the standard deviation in T_f' is found to be ±0.5 K for the 62 nm film sample based on 29 "unaged" runs. A similar value is obtained for the bulk sample based on five heating runs for four different samples made after cooling at 30 K/min. Multiple runs were not made on the 38 nm sample.

The DSC temperature was calibrated with indium and a liquid crystal CE-3 ((+)-4-*n*-hexyloxyphenyl-4′-(2′-methylbutyl)-biphenyl-4-carboxylate) at 10 and 30 K/min; the isothermal temperature calibration, which is relevant for the step scan experiments and for setting the aging temperature T_a, was performed at 0.1 K/min, which was found in other work[43] to be equivalent to performing an isothermal calibration. The absolute heat capacity was calibrated using sapphire.

Modeling Methodology

The TNM model[40–42] describes the change in fictive temperature with thermal history. In the model, the Kohlarausch-William-Watts (KWW) stretched exponential function[51] is used to describe the nonexponentiality of the relaxation, whereas the nonlinearity parameter, x, represents relative degree of dependence of relaxation time between temperature and structure (fictive temperature):

$$\ln\tau = \ln A + \frac{x\Delta h}{RT} + \frac{(1-x)\Delta h}{RT_f} \qquad (2)$$

where A is a constant, Δh is the apparent activation energy, and T_f is the fictive temperature. As shown in eq 2, the TNM model assumes an Arrhenius temperature dependence of relaxation

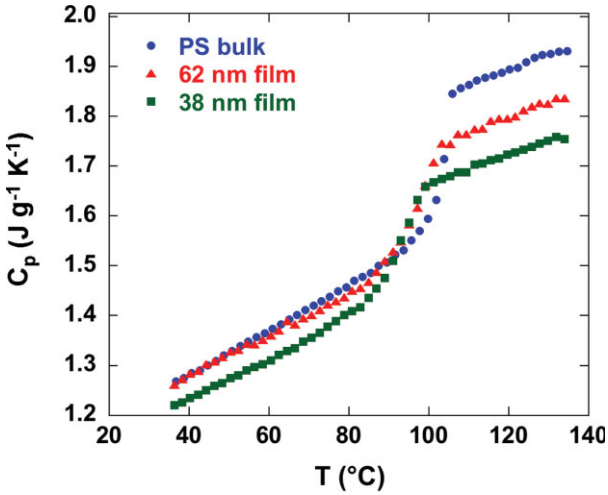

Figure 1. Absolute heat capacity versus temperature for bulk and stacked ultrathin film samples from step-scan DSC measured on heating after cooling at 30 K/min from 135 °C.

time instead of generally accepted Williams-Landell-Ferry (WLF)/Vogel-Tammann-Hess-Fulcher (VTHF)[52,53] dependence; however, for a limited temperature range around the nominal T_g, the Arrhenius approximation is valid.[24,43–47] In the TNM model, the evolution of the fictive temperature during a DSC heating scan after either cooling or isothermal aging is calculated by eq 3 as follows:

$$T_f = T_0 + \sum_i \Delta T_i \left[1 - e^{-\left(\int_0^t \frac{dT}{\tau}\right)^{\beta}}\right] \quad (3)$$

where T_0 is the initial temperature. The calculation must be started with the material in the equilibrium state above T_g, and the entire thermal history is modeled. The DSC curves are normalized to give a normalized heat capacity, which is related to dT_f/dT:

$$C_{pN} = \frac{C_p(T) - C_{pg}(T)}{\Delta C_p(T_f)} = \frac{dT_f}{dT} \quad (4)$$

DSC heating curves are each fit individually using the Marquardt algorithm.[54] In addition, T_f versus aging time data is also fit simultaneously using this algorithm. The values of the parameters, β, x, and A, are obtained from the fits, whereas $\Delta h/R$ is held constant at the value obtained from the cooling rate experimental data: 124,000 kK for the bulk and 99,500 kK for the 62 nm stacked ultrathin film sample, as shown later. The step size of temperature for the iteration is 0.1 K to minimize error during the fitting process.[47]

RESULTS

The absolute heat capacities of our stacked polystyrene samples composed of 62 nm and 38 nm films are compared with that of bulk polystyrene in Figure 1. The stacked ultrathin films show remarkable depressions of the absolute heat capacity from the bulk values in both liquid and glassy states. Interestingly, a greater depression is found in the liquid state than in the glass state; as a result, the step change in C_p at the glass transition, ΔC_p is reduced. Similar behavior, in terms of the change C_p, was reported by us previously.[23] Ellipsometry[7,21] and dielectric[14] work on polystyrene ultrathin films shows similar results for the thermal expansion coefficient (α) at the nanoscale: a greater depression of α in the liquid state compared with that in the glass, and a corresponding reduction of the step change in α at the glass transition compared with the bulk. Temperature modulated DSC measurements of

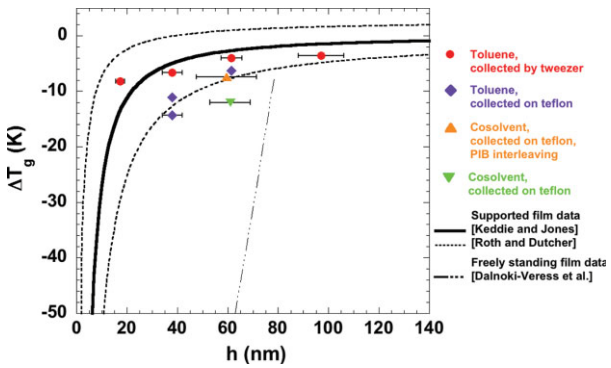

Figure 2. T_g of polystyrene ultrathin films as a function of film thickness from heating using step-scan after cooling from 135 °C at 10 K/min. Data from ref. 23 are reanalyzed using the half-height method because the half-width method was inadvertently used in that work. Symbols are shown in the legend; the solvent indicates spin-coating solution solvent; see ref. 23 for details of film preparation. The thick line is the best fit found in ref. 4 for supported polystyrene thin films. The dotted thick lines are the best fits of lower and upper limits of the data reported in ref. 5 for supported polystyrene thin films. The dash-dot line is from ref. 6 for freely standing polystyrene thin films having a similar molecular weight to our sample.

Table 1. Summary of Film Thickness Effects on ΔC_p, T_g, $T_g - T_{g\ bulk}$ from Step-Scan Measured on Heating After Cooling at 30 K/min from 135 °C for Different Film Preparation Methods[a]

Film Preparation	Film Thickness (nm)[b]	ΔC_p (J g^{-1} K^{-1})	T_g[c] (°C)	$T_g - T_{g\ bulk}$ (°C)
None (bulk)	∞	0.277	103.8 ± 0.2	0.0
Spin coated from a toluene solution,	97.0 ± 9.0	0.271	100.2	−3.6
floated onto water, and collected using tweezers	61.5 ± 4.1	0.258	99.8	−4.0
	38.0 ± 4.0	0.246	97.2	−6.6
	17.3 ± 1.7	0.223	95.6	−8.2
Toluene solution; collected on Teflon	61.5	0.211	97.5	−6.3
	38.0	0.202	92.7	−11.1
	38.0 ± 4.0	0.218	89.5	−14.3
Cosolvent solution; collected on Teflon; PIB interleaving	59.5 ± 12.0	0.183	96.4	−7.4
Cosolvent solution; collected on Teflon	61.0 ± 8.0	0.205	91.8	−12.0

[a] Values of ΔC_p, T_g, and $T_g - T_{g,bulk}$ include new data and data from ref. 23 recalculated using the half-height method; data originally reported in ref. 23 were inadvertently calculated using the half-width method.
[b] When reported, the mean and standard deviation for film thickness are based on three measurements; when based on spin-coating concentration, only the nominal value is reported.
[c] The standard deviation for the bulk T_g is based on measurements for five different samples.

oligomeric propylene glycol and oligomeric methylphenylsiloxane also show decreases in ΔC_p upon confinement in nanopores.[26,55,56]

In addition to the changes in the absolute heat capacity and in ΔC_p, the value of T_g, determined by the half-height method from the absolute heat capacity data, also decreases in the stacked ultrathin films. T_g is 103.8 °C for the bulk sample and decreases to 97.5 °C for the 62 nm and 92.7 °C for the 38 nm stacked ultrathin film giving 6.3 K and 11.1 K T_g reductions, respectively. The T_g values differ slightly from our previous work,[23] being on average 2.8 ± 1.6 K higher in this work because in our previous work, T_g was inadvertently calculated as the half-width rather than the half-height value. Figure 2 shows the T_g depression for stacked polystyrene thin films as a function of film thickness for this work, along with recalculated results based on our previous work for films ranging from 17.3 to 97.0 nm spun-coated out of toluene solvents as well as toluene/acetone cosolvents and collected on teflon (as here) or with tweezers;[23] the values of T_g, ΔC_p, and ΔT_g for all of the films studied are also tabulated in Table 1 with those from our previous work recalculated using the half-height method. The data are reasonably consistent with previously reported T_g depression values for supported polystyrene ultrathin films.

As already mentioned in the introduction, the T_g depression depends on cooling rate. In this work, we examined the depression in the limiting fictive temperature, T_f', which is obtained from a DSC heating scan immediately after cooling; the limiting fictive temperature depends only on cooling rate and approximates the glass transition temperature obtained on cooling at the same rate.[47,50] Figure 3 shows the DSC heating scans from which we will obtain T_f', as a function of cooling rate from 0.01 K/min to 30 K/min for the bulk and stacked 62 nm ultrathin film samples. In these figures, we plot the normalized heat capacity, C_{pN}, which is normalized for ease of comparison such that it is 0.0 in the glassy state and 1.0 in the liquid state. For both the bulk and ultrathin film samples, the magnitude of the enthalpy overshoot increases with decreasing cooling rate as expected. However, the stacked ultrathin film shows a dramatically reduced height of the enthalpy overshoot and a broader transition region than the bulk. The calculation results from TNM modeling are also shown in Figure 3 as dotted lines. The TNM model describes the bulk polystyrene DSC heating curves well, whereas the model shows more deviation from the data for the stacked ultrathin film sample. Nevertheless, the parameter β of the TNM model decreases in the stacked ultrathin films, consistent with a broadening of the relaxation time distribution in the ultrathin films. The TNM modeling results will be further summarized and discussed later.

The dependence of T_f' on cooling rate is shown in Figure 4. As expected, T_f' decreases with

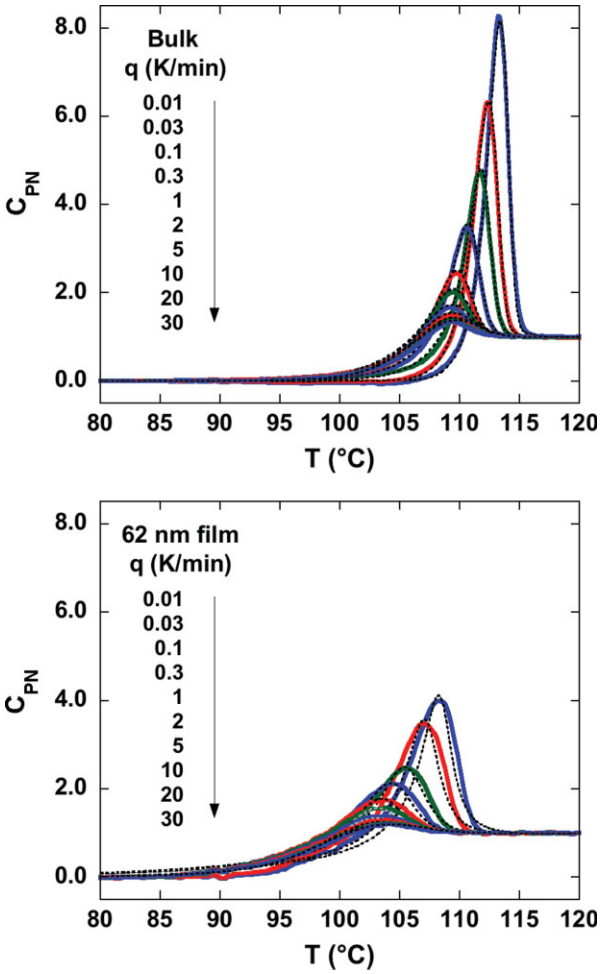

Figure 3. Normalized heat capacities as a function of cooling rate for the bulk (upper figure) and for stacked 62 nm ultrathin films (lower figure). The dotted lines are the results of TNM model fitting. [Color figure can be viewed in the online issue, which is available at www.interscience.wiley.com.]

decreasing cooling rate. In addition, the dependence of T_f' on cooling rate increases with decreasing film thickness in the stacked ultrathin film samples, yielding larger T_f' depressions at lower cooling rates for the thinner films, in agreement with other researchers.[7,26] For the 38 nm film, T_g depressions are 13.8 K and 10.3 K at cooling rates of 0.01 K/min and 30 K/min, respectively. These results also support the supposition[7] that the lack of a T_g reduction in nanocalorimetry[18,19] and AC calorimetric studies[20] is attributable to the very fast cooling rates and high frequencies used in those methods. Also shown in Figure 4 as open symbols, the values of T_g obtained from the step scan method after cooling at 30 K/min are in reasonable agreement with those of T_f' obtained from a normal scan on heating at 10 K/min also after cooling at the same rate. The values of T_f' can be compared with the step-scan T_g also in Table 2. We note that standard deviations are only reported for T_f' and T_g values in Table 2 when multiple measurements were made.

Quantitatively, the 62 nm and 38 nm stacked ultrathin films show 20 and 42% stronger cooling rate dependence of T_f' than the bulk, as calculated from the slopes in Figure 4. This dependence can also be quantified by calculating the apparent normalized activation energy, $\Delta h/R$, and the fragility index, m:[57,58]

$$\frac{\Delta h}{R} = -\frac{\mathrm{d}\ln q}{\mathrm{d}(1/T_f')} \tag{5}$$

$$m = -\frac{\mathrm{d}\log\tau}{\mathrm{d}(T_g/T)} \tag{6}$$

where q is the cooling rate, and m is the fragility index. The stacked ultrathin film samples show a lower activation energy and lower fragility than bulk, indicating a weaker temperature dependence (higher cooling rate dependence) and a stronger glass-forming liquid, in the Angell sense.[58] The values of $\Delta h/R$ and m are tabulated in Table 2. Fukao and Miyamoto[13] also reported that the fragility index from dielectric spectroscopy

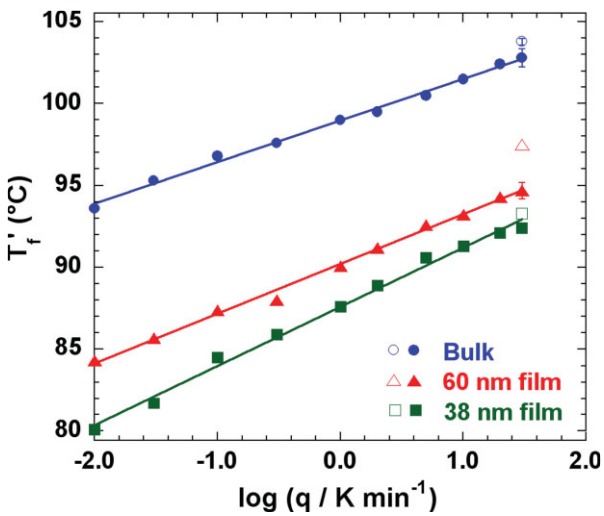

Figure 4. Cooling rate (q) dependence of the limiting fictive temperature (T_f') for bulk and ultrathin film samples. Filled symbols represent T_f' obtained from a normal DSC heating scan and open symbols represent T_g obtained from the step-scan method. [Color figure can be viewed in the online issue, which is available at www.interscience.wiley.com.]

Table 2. The Apparent Activation Energy and Fragility for Bulk Polystyrene and for 62 nm and 38 nm Stacked Ultrathin Films

Sample	T_g (°C)[a]	T_f' (°C)[b]	$\Delta h/R$ (kK)	m
Bulk	103.8 ± 0.2	102.8 ± 0.5	124	144
62 nm film	97.5	94.6 ± 0.5	99	118
38 nm film	92.7	92.4	81	98

[a] T_g from step scan on heating after cooling at 30 K/min. The standard deviation is based on five different samples of previous work.[23]

[b] T_f' from a normal heating scan at 10 K/min after cooling at 30 K/min. The standard deviation is based multiple runs on one 62 nm film sample and for the bulk, on four different bulk samples.

decreases with decreasing film thickness in supported polystyrene ultrathin films, consistent with our results. Furthermore, the values of activation energies of Fakhraai and Forrest[7] supported polystyrene films are in good agreement with our stacked ultrathin film results although the molecular weight of polystyrene in Fakhraai's work was 641,000 g/mol. Indeed, the T_g depression of our stacked ultrathin film is similar to that of the supported ultrathin films rather than that of the freely standing unsupported ultrathin films because after annealing our interfaces are assumed to be neutral polystyrene/polystyrene interfaces rather than polymer/air free surfaces.[23] The similarity of activation energy and fragility index to supported ultrathin films, therefore, provides further evidence that the free surface is not the reason for the T_g depression in our stacked ultrathin films.

As shown in Figure 3, slow cooling results in more relaxation during cooling and, hence, higher enthalpy overshoots and lower values of the limiting fictive temperature compared with a faster cooling rate. Similarly, isothermal structural relaxation or physical aging results in larger overshoots and lower fictive temperatures as aging time increases. Figure 5 shows the DSC heating scans as a function of aging time for the bulk and the 62 nm ultrathin film samples for an aging temperature (T_a) 5 K below the respective nominal T_g of each sample as measured with step scan. Again, we plot the normalized heat capacity, C_{pN}, for ease of comparison. As aging time increases, the magnitude of the enthalpy overshoot increases, as expected. However, similar to the DSC scans after cooling at various rates, the stacked ultrathin film sample shows a reduced height of the enthalpy overshoot and a broader transition than the bulk for a given aging time; this is also similar to the DSC results observed for small molecules confined in nanopores after aging[27] and similar to the early results of Kawana and Jones.[21] The TNM model calculations are also shown as dotted lines in Figure 5. Similar to Figure 3, the fit is better for the bulk sample.

The evolution of the fictive temperature (T_f) as a function of aging time can be calculated from the data shown in Figure 5, and this is shown in Figure 6 along with similar data for other aging temperatures. For ease of comparison, we plot the difference between the fictive temperature and the aging temperature ($T_f - T_a$) versus the logarithm of the aging time. The fictive temperature decreases nonexponentially as a function aging time, leveling off at equilibrium at a value where $T_f = T_a$; note that this differs from the case of aging in nanopore confinement[27] where the 3-D constraints result in isotropic tensile stresses such that the equilibrium value of T_f does not equal T_a. The time required to reach equilibrium also increases as the aging temperature decreases. Comparing the physical aging behavior between the bulk and ultrathin film samples, the evolution of the fictive temperature and the rate of aging appears to be very similar for aging a given distance from each sample's T_g. However, since T_g is lower in the ultrathin film sample, at the same temperature, the stacked ultrathin film shows an acceleration of physical aging.

The TNM model is able to describe the evolution of the fictive temperature with aging very well, and the fit is also shown in Figure 6. However, despite the similarity in the shape of the curves, large differences are found in TNM parameters for the bulk and stacked ultrathin film samples. The nonexponential parameter, β, is 0.807 for the bulk and 0.566 for the stacked ultrathin film sample, respectively, indicating that the

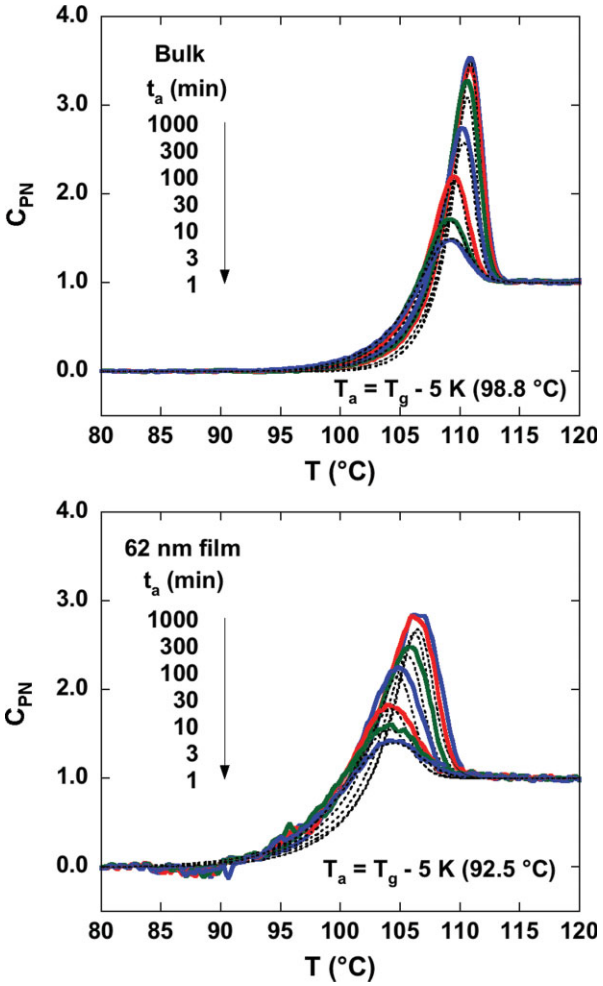

Figure 5. Normalized heat capacities as a function of the aging time at the aging temperature of T_g – 5 K for the bulk (upper figure) and for the stacked 62 nm ultrathin film sample (lower figure). The dotted lines are the results of TNM model fitting. [Color figure can be viewed in the online issue, which is available at www.interscience.wiley.com.]

stacked ultrathin film has a wider distribution of relaxation times.

DISCUSSION

The TNM model was fit to three types of data for both bulk and stacked ultrathin film samples: DSC heating scans after cooling at various rates, DSC heating scans after aging isothermally at various times, and fictive temperature versus aging time data at various isothermal temperatures. In all cases, the parameter β was smaller for the ultrathin films indicating a broadened relaxation time distribution. However, as shown in Table 3, the TNM model parameters obtained from fitting the three sets of data are quantitatively different, and for one data set, x decreases for the stacked ultrathin films, whereas for the other sets, it increases relative to the bulk value. In fact, the TNM model has documented shortcomings, including the inability to describe multiple data sets and to capture thermal history with one set of parameters, the lack of physical meaning of x, and a mutual dependence of β

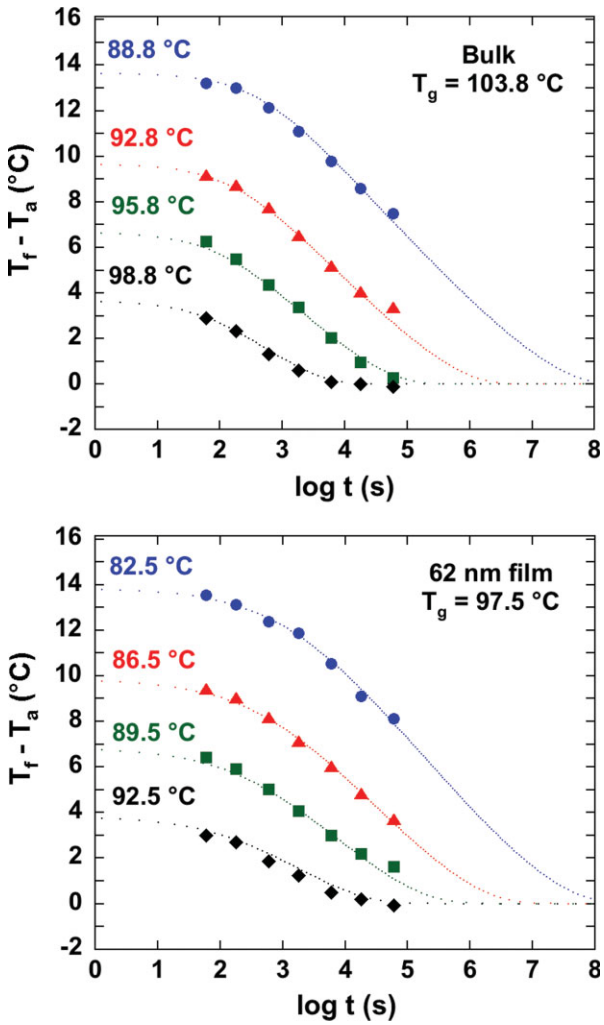

Figure 6. Evolution of fictive temperature during isothermal aging for the bulk (upper figure) and for the stacked 62 nm ultrathin film sample (lower figure) at the same distance from T_g: (●) $T_a = T_g - 5$ K, (▲) $T_a = T_g - 8$ K, (■) $T_a = T_g - 11$ K, (◆) $T_a = T_g - 15$ K. The dotted lines are the results of TNM model fitting. [Color figure can be viewed in the online issue, which is available at www.interscience.wiley.com.]

Table 3. TNM Model Parameters of β and x for Fitting Different Data Sets

	Bulk		62 nm Film	
Data Set	β	x	β	x
C_{pN} vs. T as a $f(q)$	0.482 ± 0.250	0.759 ± 0.121	0.285 ± 0.050	0.471 ± 0.355
C_{pN} vs. T as a $f(t_a)$				
$T_a = T_g - 5$ K	0.523 ± 0.104	0.675 ± 0.079	0.371 ± 0.022	0.553 ± 0.176
$T_a = T_g - 8$ K	0.443 ± 0.054	0.503 ± 0.158	0.340 ± 0.028	0.549 ± 0.280
$T_a = T_g - 11$ K	0.403 ± 0.072	0.456 ± 0.208	0.348 ± 0.060	0.599 ± 0.311
$T_a = T_g - 15$ K	0.364 ± 0.052	0.437 ± 0.240	0.337 ± 0.092	0.768 ± 0.315
T_f vs. t_a	0.807 ± 0.05	0.308 ± 0.06	0.566 ± 0.05	0.415 ± 0.06

and x.[24,47,48,59–61] Nevertheless, the nonexponentiality parameter β for all three sets of data is lower for the stacked ultrathin films, which indicates that an increased distribution of relaxation times and a broadening of the glass transition is a distinct characteristic of nanoconfinement. Our stacked ultrathin film sample also shows a lower value of the fragility index (i.e., it is a stronger glass former as shown in Table 2) than the bulk despite its lower value of β (i.e., increased heterogeneity). Our observed positive correlation between fragility and nonexponentiality in confined geometry is inconsistent with the typical inverse correlation reported in the literature,[62] but it is consistent with the results from other researchers studying supported polystyrene ultrathin films.[13,14]

Compared with the bulk polystyrene sample, the sample of stacked 62 nm films shows a reduced height of the enthalpy overshoot and a broader transition for a given thermal history, as shown in both Figures 3 and 5. However, although the enthalpy overshoots have considerably different shapes, the evolution of $T_f - T_a$ for the stacked ultrathin film seems to be the same as that of the bulk as shown Figure 6 for aging a given distance from T_g. To investigate the physical aging rate more quantitatively, the time required to reach equilibrium (t_∞) is calculated as a function of the aging temperature and is plotted versus $T_g - T_a$ in Figure 7 to account for the difference in T_g between the ultrathin film and bulk samples. Compared with the bulk, the stacked ultrathin film shows slightly longer times required to reach equilibrium when aged a comparable distance below T_g in the temperature range that we studied (near T_g). However, the slope of the t_∞ versus $T_g - T_a$ is 17% lower for the stacked ultrathin film sample such that below approximately $T_a = T_g - 15$ K, the films are expected to come to equilibrium faster than the bulk when aged at the same distance from T_g. This difference in slopes is quantitatively consistent with the higher cooling rate dependence (weaker temperature dependence) shown in Figure 4. The inset in Figure 7 shows the comparison between the time required to reach equilibrium as a function of aging temperature; at any given aging temperature, the ultrathin film sample reaches equilibrium faster than the bulk sample.

Another way to quantify the differences in aging between the ultrathin films and the bulk is to define an aging rate. In volumetric measurements, the physical aging rate was calculated from the slope of the specific volume versus logarithmic aging time curve since the specific volume varies linearly with log t_a during aging.[63] Similarly, we calculate a physical aging rate (R) from the slope of Figure 6 in the linear region:

$$R = -\frac{dT_f}{d\log t_a} \tag{7}$$

In eq 7, the units of R are K per decade and the minus sign is introduced to make the quantity positive. As shown in Figure 8, the physical aging rate increases from 1.6 K/decade for small temperature jumps (high aging temperatures) to ~2.4 K/decade for large temperature jumps. However, the physical aging rates of the bulk and 62 nm ultrathin film are similar for aging a given distance below T_g, with perhaps a slightly higher aging rate for the bulk at the highest temperatures very near T_g. The standard errors of the aging rate (σ_R) in Figure 8 were calculated from the error in the T_f measurement[64]:

$$\sigma_R = \frac{\sigma_{T_f}}{\sqrt{\sum \log t_i^2}} \tag{8}$$

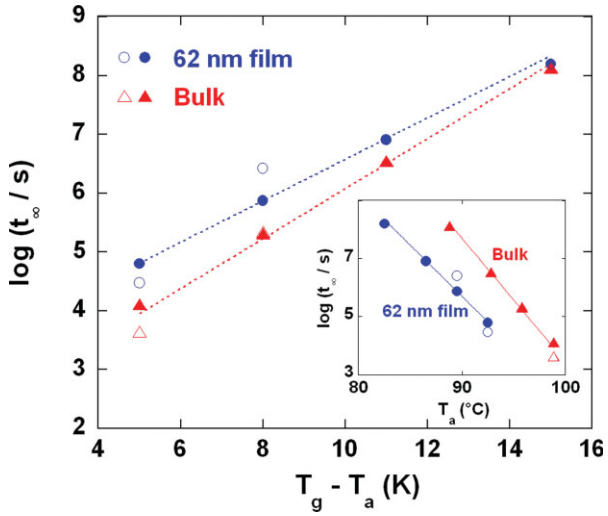

Figure 7. The time to reach equilibrium versus the size of the temperature down jump for bulk and 62 nm ultrathin film samples. Filled symbols represent the values obtained from TNM model, and open symbols represent the values obtained from KWW fitting near equilibrium. The inset shows the time to reach equilibrium versus the aging temperature. [Color figure can be viewed in the online issue, which is available at www.interscience.wiley.com.]

where σ_{Tf} is the standard error of the measured fictive temperature (0.5 K), and t_i is the corresponding aging time to each fictive temperature data.

The inset in Figure 8 shows the aging rate R as a function of aging temperature. In this comparison, the ultrathin film sample shows a lower aging rate than the bulk at a given aging temperature for the aging temperatures studied presumably because of the depressed T_g of the ultrathin film and the smaller driving force to reach equilibrium. Priestley et al.[29] found a similar result when aging below the bulk T_g but above T_g of an ultrathin polystyrene film supported on quartz although in that case the ultrathin film did not age at all because it was in equilibrium. When aging the same samples 71 K below the bulk T_g (i.e., at 29 °C) for aging times to 4800 s, Priestley et al.[29] reported that the aging rate was considerably lower for the ultrathin film sample; however, it is not clear that the linear decay region (where, for example, volume decreases linearly with the logarithm of time) can be accurately determined in 4800 s for aging so far below T_g—see for example, Figure 6 where we would be hard pressed to obtain a rate from the linear decay region for aging 15 K below T_g if we had data only to 4800 s. Greiner and Schwarzl[63] have argued that reaching the linear decay region is necessary for calculating a meaningful aging rate. On the other hand, Huang and Paul[30,31] found that the aging rate at temperatures more than 130 K below T_g increased for thin (micron-size) films and that the aging rate decreased with decreasing temperature. Although these findings seem to be inconsistent with our results, we suggest that the difference may be due to the different temperature ranges of the studies. Greiner and Schwarzl[63] showed that for a sufficiently wide range of aging temperature, the aging rate increases with decreasing aging temperature near T_g, reaches a maximum aging rate, and then decreases as the aging temperature decreases further. We are in the regime close to T_g where the aging rate is increasing with decreasing temperature, whereas Huang and Paul's study was done in the regime far from T_g.

More importantly, however, we argue that the aging rate near T_g is not necessarily indicative of whether aging is accelerated or not because in this regime, the aging rate depends both on the distance from T_g (the driving force) and the temperature. In other words, a low aging rate can indicate either that the material is very close to equilibrium (such that the aging rate does not reflect the relaxation time) or that the relaxation time is long. We showed that the times required

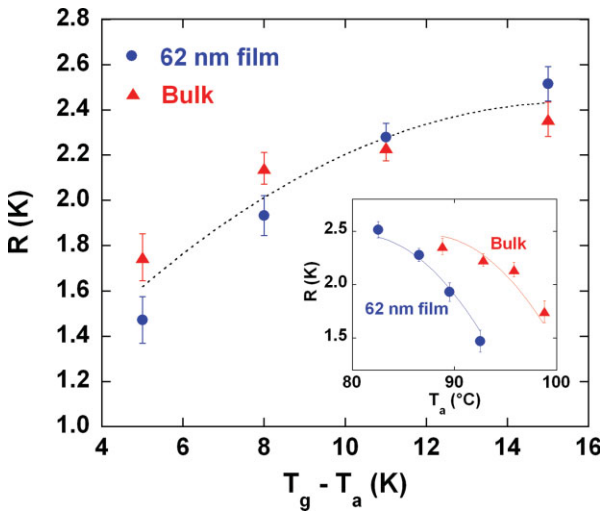

Figure 8. The aging rate ($R = -dT_f/d\log t_a$) versus the size of the temperature down jump for bulk and 62 nm ultrathin film samples. The aging rates were calculated from the slope of T_f versus log t_a in the linear region. The inset shows the aging rates versus the aging temperature. Lines are guides for the eye only. [Color figure can be viewed in the online issue, which is available at www.interscience.wiley.com.]

to reach equilibrium are significantly lower for the ultrathin film samples compared with the bulk at a given aging temperature - indicating that aging is accelerated. Hence, the fact that the aging rate is lower for the thin films at a given aging temperature simply indicates that the samples are closer to equilibrium, and it does not indicate that the relaxation times are longer.

CONCLUSIONS

The effects of ultrathin film confinement on the glass transition of polystyrene and its kinetics, including structural recovery, were investigated by DSC using stacked ultrathin film samples. Measurements were made of the fictive temperature as a function of cooling rate and as a function of aging time at various isothermal aging temperatures. The reduced height of the enthalpy overshoot and the broadened transition in DSC heating scan curves are found to be characteristics of ultrathin film confinement and seem to result from a broadened distribution of relaxation times, as supported by a decrease of the TNM model parameter β for the ultrathin film sample. The limiting fictive temperature of the ultrathin film sample increases more than that of the bulk sample with increasing cooling rate, such that the magnitude of T_g depression decreases with increasing cooling rate, and the apparent activation energy and fragility decrease for the thin films. At high enough cooling rates, no T_g depression may exist in agreement with other researchers in the field. In addition, the enthalpy relaxation of the ultrathin film sample shows similar behavior to the bulk for aging at the same distance below T_g, as shown in terms of the time to reach equilibrium and the physical aging rate. However, at a given aging temperature, acceleration of physical aging in terms of the time required to reach equilibrium is observed in the ultrathin film sample presumably because it is closer to T_g due to the T_g depression in the ultrathin film sample. For aging in the regime near T_g, the aging rate is not a good indicator of whether or not aging is accelerated.

The authors gratefully acknowledge funding from NSF DMR 0304640.

REFERENCES AND NOTES

1. Alcoutlabi, M.; McKenna, G. B. J Phys Condens Matter 2005, 17, R461–R524.
2. Forrest, J. A.; Jones, R. A. L. In Polymer Surface Interfaces and Thin Films; Karim, A.; Kumar, S., Eds.; World Scientific: Singapore, 2000.
3. Alba-Simionesco, C.; Coasne, B.; Dosseh, G.; Dudzidak, G.; Gubbins, K. E.; Randhakrishnan, R.; Silininska-Bartkowiak, M. J Phys Condens Matter 2006, 18, R15–R68.
4. Keddie, J. L.; Jones, R. A. L. Israel J Chem 1995, 35, 21–26.
5. Roth, C. B.; Dutcher, J. R. J Electroanal Chem 2005, 584, 13–22.
6. Dalnoki-Veress, K.; Forrest, J. A.; Murray, C.; Cigault, C.; Dutcher, J. R. Phys Rev E 2001, 63, 031801-1–031801-10.
7. Fakhraai, Z.; Forrest, J. A. Phys Rev Lett 2005, 95, 025701-1–025701-4.
8. Tsui, O. K. C.; Russell, T. P.; Hawker, C. J. Macromolecules 2001, 34, 5535–5539.
9. Ellison, C. J.; Torkelson, J. M. Nature Mater 2003, 2, 695–700.
10. Hutcheson, S. A.; McKenna, G. B. Phys Rev Lett 2005, 94, 076103-1–076103-4.
11. Wang, X. R.; Zhou, W. S. Macromolecules 2002, 35, 6747–6750.
12. DeMaggio, G. B.; Frieze, W. E.; Gidley, D. W.; Zhu, M.; Hristov, H. A.; Yee, A. F. Phys Rev Lett 1997, 78, 1524–1527.
13. Fukao, K.; Miyamoto, Y. Phys Rev E 2001, 64, 011803-1–011803-9.
14. Fukao, K.; Miyamoto, Y. Phys Rev E 2000, 61, 1743–1754.
15. Ellison, C. J.; Kim, S. D.; Hall, D. B.; Torkelson, J. M. Eur Phys J E 2002, 8, 155–166.
16. O'Connell, P. A.; McKenna, G. B. Science 2005, 307, 1760–1763.
17. Soles, C. L.; Douglas, J. F.; Wu, W.; Peng, H.; Gidley, D. W. Macromolecules 2004, 37, 2890–2900.
18. Efremov, M. Y.; Olson, E. A.; Zhang, M.; Allen, L. H. Phys Rev Lett 2003, 91, 085703-1–085703-4.
19. Efremov, M. Y.; Olson, E. A.; Zhang, M.; Allen, L. H. Macromolecules 2004, 37, 4607–4616.
20. Lupascu, V.; Huth, H.; Schick, Ch.; Wubbenhorst, M. Thermochim Acta 2005, 432, 222–228.
21. Kawana, S.; Jones, R. A. L. Eur Phys J E 2003, 10, 223–230.
22. Priestley, R. D.; Broadbelt, L. J.; Torkelson, J. M.; Fukao, K. Phys Rev E 2007, 75, 061806-1–061806-10.
23. Koh, Y. P.; McKenna, G. B.; Simon, S. L. J Polym Sci Part B: Polym Phys 2006, 44, 3518–3527.
24. Hodge, I. M. J Non-Cryst Solids 1994, 169, 211–266.
25. Qin, Q.; McKenna, G. B. J Non-Cryst Solids 2006, 352, 2977–2985.
26. Schönhals, A.; Goering, H.; Schick, Ch.; Frick, B.; Zorn, R. J Non-Cryst Solids 2005, 351, 2668–2677.
27. Simon, S. L.; Park, J. Y.; McKenna, G. B. Eur Phys J E 2002, 8, 209–216.

28. Priestley, R. D.; Ellison, C. J.; Broadbelt, L. J.; Torkelson, J. M. Science 2005, 309, 5733, 456–459.
29. Priestley, R. D.; Broadbelt, L. J.; Torkelson, J. M. Macromolecules 2005, 38, 654–657.
30. Huang, Y.; Paul, D. R. Polymer 2004, 45, 8377–8393.
31. Huang, Y.; Paul, D. R. Macromolecules 2005, 38, 10148–10154.
32. Bansal, A.; Yang, H.; Li, C.; Cho, K.; Benicewicz, B. C.; Kumar, S. K.; Schadler, L. S. Nature Mater 2005, 4, 693–698.
33. Rittigstein, P.; Priestley, R. D.; Broadbelt, L. J.; Torkelson, J. M. Nature Mater 2007, 6, 278–282.
34. Lu, H.; Nutt, S. Macromol Chem Phys 2003, 204, 1832–1841.
35. Lu, H.; Nutt, S. Macromolecules 2003, 36, 4010–4016.
36. Vlasveld, D. P. N.; Bersee, H. E. N.; Picken, S. J. Polymer 2005, 46, 12539–12545.
37. Khojin, A. S.; Jana, S.; Zhong, W. H. K. J Mater Sci 2007, 42, 6093–6101.
38. Lee, A.; Lichtenhan, J. D. Macromolecules 1998, 31, 4970–4974.
39. Roth, C. B.; Torkelson, J. M. Macromolecules 2007, 40, 3328–3336.
40. Moynihan, C. T.; Macedo, P. B.; Montrose, C. J.; Gupta, P. K.; DeBolt, M. A.; Dill, J. F.; Dom, B. E.; Drake, P. W.; Easteal, A. J.; Elterman, P. B.; Moeller, R. P.; Sasabe, H.; Wilder, J. A. Ann NY Acad Sci 1976, 279, 15–35.
41. Tool, A. Q. J Am Ceram Soc 1946, 29, 240–253.
42. Narayanaswamy, O. S. J Am Ceram Soc 1971, 54, 491–498.
43. Simon, S. L.; Sobieski, J. W.; Plazek, D. J. Polymer 2001, 42, 2555–2567.
44. Bernazzani, P.; Simon, S. L. J Non-Cryst Solids 2002, 307, 470–480.
45. Bernazzani, P.; Simon, S. L.; Plazek, D. J.; Ngai, K. L. Eur Phys J E 2002, 8, 201–207.
46. Li, Q.; Simon, S. L. Polymer 2006, 47, 4781–4788.
47. Badrinarayanan, P.; Zheng, W.; Li, Q.; Simon, S. L. J Non-Cryst Solids 2007, 353, 2603–2612.
48. Simon, S. L. Macromolecules 1997, 30, 4056–4063.
49. Rubinstein, M.; Colby, R. H. Polymer Physics; Oxford: New York, 2003.
50. Moynihan, C. T. In Assignment of the Glass Transition; Seyler, R. J., Ed.; ASTM: Philadelphia, 1994.
51. Williams, G.; Watts, D. C. Trans Faraday Soc 1970, 66, 80–85.
52. Williams, M. L.; Landell, R. F.; Ferry, J. D. J Am Chem Soc 1955, 77, 3701–3707.
53. Vogel, H. Phys Z 1921, 22, 645–646.
54. Marquardt, D. W. J Soc Indust Appl Math 1963, 11, 431–441.
55. Schönhals, A.; Goring, H.; Schick, Ch. J Non-Crystalline Solids 2002, 305, 140–149.
56. Schönhals, A.; Goring, H.; Schick, Ch. MRS Symp Proc 2006, 899E, 0899-N09-05.
57. Moynihan, C. T.; Easteal, A. J.; Wilder, J. J Phys Chem 1974, 78, 2673–2677.
58. Angell, C. A. J Non-Cryst Solids 1991, 131, 13–31.
59. Hodge, I. M. Macromolecules 1986, 19, 936–938.
60. Hodge, I. M. Macromolecules 1987, 20, 2897–2908.
61. Simon, S. L.; Bernazzani, P. J Non-Cryst Solids 2006, 352, 4763–4768.
62. Debenedetti, P. G.; Stillinger, F. H. Nature 2001, 410, 259–267.
63. Greiner, R.; Schwarzl, F. R. Rheol Acta 1984, 23, 378–395.
64. Bevington, P. R. Data Reduction and Error Analysis for the Physical Sciences; McGraw Hill: New York, 1969.